Optical transition in self-assembled InAs/GaAs quantum lens under high hydrostatic pressure

Arezky H. Rodríguez,[1,a)] C. Trallero-Giner,[2] C. A. Duque,[3] and G. J. Vázquez[4]
[1]*Academia de Matemáticas, Universidad Autónoma de la Ciudad de México, Mexico City 03020, Mexico*
[2]*Facultad de Física, Universidad de La Habana, 10400 C. Habana, Cuba*
[3]*Instituto de Física, Universidad de Antioquia, AA 1226 Medellín, Colombia*
[4]*Instituto de Física, Universidad Nacional Autónoma de México (UNAM), Apdo. Postal 20-364, San Ángel, México D.F. 01000, Mexico*

(Received 7 October 2008; accepted 4 January 2009; published online 23 February 2009)

We present a simulation to characterize the dependence on hydrostatic pressure for the photoluminescence spectra in self-assembled quantum dots with lens shape geometry. We have tested the physical effects of the band offset and electron-hole effective masses on the optical emission in dot lens. The model could be implemented to get qualitative information of the parameters involved in the quantum dot or the measured optical properties as function of pressure.
 [DOI: 10.1063/1.3078109]

I. INTRODUCTION

The study of the physical properties of nanostructures is of great importance nowadays. Specifically, self-assembled quantum dots (QDs) grown by Stranski–Krastanov method have attracted great attention from the scientific community.[1,2] A lot of works have been devoted to the study of the electronic and optical properties of QDs where their shapes are modeled as quantum pyramids.[3–10] It has also been considered as QDs having lens shape.[11–20] In this case, there is a rather extended opinion which states that the work done considering QDs with pyramid shapes can be straightforwardly applied to characterize the QDs with lens shape and therefore the calculation made in pyramid QDs does not need to be recalculated in quantum lenses. Nevertheless, different authors have shown the importance of considering the full lens geometry for a better description of the optical properties of the QDs.[21–23]

Photoluminescence (PL) measurement under high hydrostatic pressure has been proved to be an effective tool in exploring the electronic structure and optical transitions in QDs.[24–31] A significant decrease in the hydrostatic pressure coefficient (PC) for InAs/GaAs QDs in comparison with bulk material is reported. Different experimental works have proposed some explanations: nonuniform indium distribution in the QDs,[32] pressure dependence of the effective masses and confined potential,[31] and the necessity to include a nonlinear strain distribution[25] and band-gap pressure dependence and finite barriers.[27] From the theoretical point of view some works have been devoted to explain the obtained low value of hydrostatic PC. For example, elasticity theory in Ref. 24, atomistic empirical pseudopotential method in Ref. 27, and atomistic valence-force field method in Ref. 26 were implemented. In all of the previous works, the QDs have been modeled as quantum pyramids.

The motivation of the presented work is focused on the experimental observations of Refs. 25 and 28–30. They have performed studies of low-temperature PL in InAs and InGaAs self-assembled quantum dots (SAQDs) embedded in GaAs matrix under hydrostatic pressure. From the pressure dependence of the main electron-hole transition energy, a PC of 20% smaller than the InAs case was reported. In Refs. 24 and 28 some arguments could explain this difference in the pressure coefficients: (i) the change in the band offset between InAs and GaAs, (ii) the strong tension in the InAs SAQD material, and (iii) the lowering of the electron and light hole quantization energies due to the change in the effective masses with pressure.

In Ref. 30 Itskevich *et al.* argued that the dots can be characterized by a lens symmetry with a base between 7.5 and 10.6 nm of radius and ratio height/radius between 0.28 and 0.4. We need to appoint that, in general, the shape and dimensions of the InAs/GaAs SAQDs are not always well determined and a degree of freedom remains.

An attempt to describe the PL peak energies can be found in Ref. 33 where the spatial confined geometry was modeled as a parabolic cylinder potential avoiding the specific geometry of the SAQDs. It is well known that different geometries yield different results, as shown in Ref. 23 when comparing the electronic properties between a cylindrical and a lens shape SAQD. In this paper, the QD will be modeled by a full lens symmetry with maximum height b and circular cross section of radius a with $b<a$. A model that allows the inclusion of the finite barrier effect in SAQD with lens shape is implemented. The model allows to validate the importance of the change in the band offset and electron-hole effective masses as a function of pressure on the PL spectra. In our simulation the strain effect within the QD has been taken into account through an effective linear PC at zero temperature which considers the built-in strain of the dot by assuming a simple two-dimensional strained layer model (see Table I and Refs. 31, 33, and 34). The QDs considered here are within the strong confinement regime and as first approximation the excitonic effects are ignored.

The remainder of this paper is organized as follows. Section II deals with the general trends of the simulation for

[a)]Electronic mail: arezky@gmail.com.

TABLE I. Values of the parameters used in the calculation of the energy levels for the InAs/GaAs quantum lens under pressure. The symbol * means that the tension effect of the InAs embedded in the GaAs matrix was taken into account.

	InAs	GaAs
$E_g^{(o)}$ (eV)	0.533[a,*]	1.519[a]
α (meV/kbar)	7.7[b,*]	10.8[c]
κ ($\times 10^{-4}$ eV/K)	2.76[a]	5.405[a]
c (K)	83[a]	204[a]
γ_1	20.4[d]	6.85[e]
γ_2	8.37[d]	2.1[e]
δ (meV)	380[d]	341[d]
$2(P_o^2/m_o)$ (eV)	19[d]	12.9[f]

[a]Reference 42.
[b]Reference 43.
[c]Reference 33.
[d]Reference 44.
[e]Reference 45.
[f]Reference 46.

including the hydrostatic pressure in QDs characterized by a lens geometry with a short discussion of the model used to obtain the electronic spectrum. Section III presents theoretical calculations for the system by comparing the effect of the hydrostatic pressure over different quantum lenses. A comparison with available PL data of the main transition energy as a function of P is presented in Sec. IV. Finally, Sec. V is devoted to the conclusions.

II. BASIC RELATIONS

The fractional change in volume in the InAs domain is given by

$$\delta V/V = -3P(S_{11}+2S_{12}), \tag{1}$$

where $S_{11}=1.946\times10^{-3}$ kbar^{-1} and $S_{12}=-6.855\times10^{-4}$ kbar^{-1} are the compliance constants.[33] The energy gap E_g at low temperature at the Γ point is proportional to the pressure according to

$$E_g(P,T) = E_g^{(o)} + \alpha P - \frac{\kappa T^2}{T+c}, \tag{2}$$

where $E_g^{(o)}$ is the gap energy at $T=0$ and $P=0$, α is the pressure coefficient, and κ and c are the temperature coefficients.[35] For the case of InAs/GaAs SAQD, the parameters used for both materials are shown in Table I. With the inclusion of the finite stress it can be seen that the α coefficient is greater for the GaAs material than the InAs. Hence, the confined potential for the conduction and valence bands will increase with pressure. The variation in the effective masses was evaluated in terms of the fundamental gaps according to the Kane model and it was obtained as[36]

$$\frac{m_o}{m_e^*} = 1 + 2\left(\frac{P_o^2}{m_o}\right)\frac{E_g+\frac{2}{3}\delta}{E_g(E_g+\delta)} \tag{3}$$

for electrons,

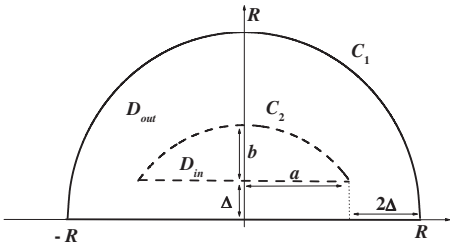

FIG. 1. Transversal section of a 3D lens D_{in} in a semispherical medium D_{out} with contours C_2 and C_1, respectively. Contours C_1 and C_2 are separated a distance equal to or greater than Δ along the perpendicular axis.

$$\frac{m_o}{m_{lh}^*} = -\left[1-\frac{4}{3E_g}\left(\frac{P_o^2}{m_o}\right)\right] \tag{4}$$

for light holes, and

$$\frac{m_o}{m_{hh}^*} = \gamma_1 - 2\gamma_2 \tag{5}$$

for the heavy holes. Here E_g is the gap energy given by Eq. (2), γ_1 and γ_2 are the Luttinger parameters, δ is the spin-orbit splitting, and m_o is the free electron mass. The parameter P_o is the interband momentum matrix element between the conduction and valence bands.

The PL lines in such QD structures are proportional to the optical transition energies $E_{N_e,m_e;N_h,m_h}(P)$ which are function of the pressure. The energy levels at a given band are characterized by the radial label N with axial projection of the angular momentum with quantum number m. Then, in the framework of the parabolic band model, the transition energy $E_{N_e,m_e;N_h,m_h}$ means the energy difference between the states (N_h,m_h) and (N_e,m_e) in the valence and conduction bands, respectively. The oscillator strength for dipole-allowed conduction-valence band transitions is proportional to the optical matrix element (OME) $d(N_e,m_e;N_h,m_h)$ given by

$$d(N_e,m_e;N_h,m_h) = \left|\int_D \Psi_{N_e,m_e;N_h,m_h}(\mathbf{r},\mathbf{r})d\mathbf{r}\right|^2. \tag{6}$$

In the case of a SAQD with axial symmetry, it is obtained for the former expression $d(N_e,m_e;N_h,m_h)=0$ for $m_e\neq m_h$ and only the terms with $m_e=m_h$ remains. The integration is over the whole domain D of the QD.

A. Electronic structure

Although previous theoretical studies in QDs with lens shape[37–39] considered infinite potential wall, the finite value of the band offset is a fundamental parameter when considering the hydrostatic pressure, as can be seen from Eq. (2). Then, in our case, the problem for a finite barrier will be modeled including a lens shape well potential with height V_o in a hard-wall semispherical region, as shown in Fig. 1. The semispherical region is divided in two regions, D_{in} and D_{out} with confined potential zero and V_o, respectively, and the mismatch boundary conditions are considered at the interface. Assuming parabolic band dispersion for electrons and holes, the solution of the effective mass equation for a lens geometry, with finite barrier, in an infinite surrounding me-

dium can be obtained by minimizing the effect of the external boundary C_1 over the wave function of the corresponding energy level under study. This can be achieved by taking larger enough value of the distance Δ. The equation for the whole region D is

$$-\frac{\hbar^2}{2}\nabla\left(\frac{1}{m^*(r,\theta,\phi)}\nabla\Psi\right)+V(r,\theta,\phi)\Psi=E\Psi,$$

$$(r,\theta,\phi)\in D=D_{\text{in}}+D_{\text{out}}, \tag{7}$$

where

$$V(r,\theta,\phi)=\begin{cases}0 & (r,\theta,\phi)\in D_{\text{in}}\\ V_o & (r,\theta,\phi)\in D_{\text{out}}\end{cases}$$

and

$$m^*(r,\theta,\phi)=\begin{cases}m^*_{\text{in}} & (r,\theta,\phi)\in D_{\text{in}}\\ m^*_{\text{out}} & (r,\theta,\phi)\in D_{\text{out}}.\end{cases}$$

The analytical solution of Eq. (7) is sought in the closed form

$$\Psi=\sum_i C_i\Psi_i^{(o)}, \tag{8}$$

where the set of functions $\{\Psi_i^{(o)}\}$ is a complete set of functions in the three-dimensional (3D) domain D determined by the semisphere and its explicit representation can be found in Ref. 38. With the former expansion the functions Ψ satisfy the boundary condition of infinite barrier in the contour C_1 because the set of functions $\{\Psi^{(o)}\}$ does. On the other hand, Eq. (7) and the corresponding solution given by Eq. (8) are written for the whole domain D. It guarantees that the matching conditions at the contour C_2 are also satisfied, but only at those points where it is well defined the derivative of the wave function. This does not occur at the corners of the contour C_2 where the differentiation with respect to the normal to the surface presents a discontinuity and, generally speaking, the problem is then not well defined.[40] The obtained eigenvalues constitute only an estimation of the solution for the real problem but we accept this solution as a better one than the values reported by the infinite barrier case. The present formalism has been applied in previous works,[41] but not explicit analysis has been done about the method used and the fulfillment of the matching conditions between the internal and the external domain.

In order to visualize the results of the above described model, two different quantum lens geometries of InAs/GaAs have been considered. In Fig. 2 are shown the first five electronic levels as a function of the lens radius. Panel (a) is for $b/a=0.91$ while panel (b) is for $b/a=0.51$. The levels calculated within the hard-wall model[38] are shown by dotted lines while the results obtained using the finite barrier model are described by solid lines. For the finite barrier case, a 500 $\times$500 matrix and a value of $\Delta/R=0.3$ have been used to guarantee that the absolute and relative errors introduced by the contour C_1 and the cutoff of Eq. (8) in the values obtained for the energy levels are less than 10^{-3}. According to the results of Fig. 2, it can be seen that the infinite barrier is a good approximation for radius of the order of 20 nm or higher when $b/a=0.91$. As b/a decreases, the values of the energy levels increase and the effects of the finite barrier become important. Then, it is necessary to consider the finite barrier effects to get better accuracy for the energy level distribution at the same range of radius.

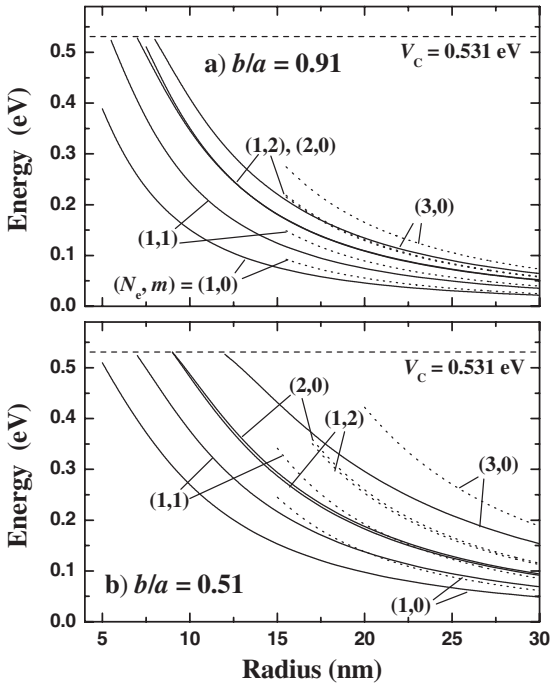

FIG. 2. First five electronic levels in the conduction band for an InAs/GaAs quantum lens as a function of the lens radius. (a) $b/a=0.91$ and (b) $b/a=0.51$. The calculation is taken as $\Delta/R=0.3$ (solid lines) for the finite barrier model. Dotted lines are the results considering the infinite potential barrier model (Ref. 38). The conduction confined potential V_c is represented by dashed lines.

III. RESULTS AND DISCUSSION

Figure 3 shows the variation with pressure of the first energy levels in the conduction band for two lens configurations $b/a=0.91$ [Fig. 3(a)] and $b/a=0.51$ [Fig. 3(b)] with $a=9$ nm. Both figures include the height of the potential barrier $V_o=V_c$ as a function of the pressure by dashed lines. The band offset of the strained InAs/GaAs quantum lens was taken, for the conduction (valence) band, as 54% (46%) of the total band difference.[33]

It is interesting to note the decrease in the values of the conduction energy levels with the increase in P, in spite of the increase in the barrier height according to Eq. (2) and the decrease in the dot radius following Eq. (1). This effect is very robust for both configurations shown in Fig. 3. This fact is a direct consequence of the strong influence of the variation in the electron mass with P according to Eq. (3). The same will happen for the light hole [see Eq. (4)]. In the case of Fig. 3(b), due to the strong lens deformation, only two electron states are present at $P=0$ [(1,0) and (1,1)] and two more appear at $P\approx 20$ kbars.

In Fig. 4 it is shown the OME as a function of the pressure for the first electron-hole states with $m=0$. Each line is labeled according to the corresponding transition $(N_e,N_h;m)$, which means a transition between the valence band states N_h

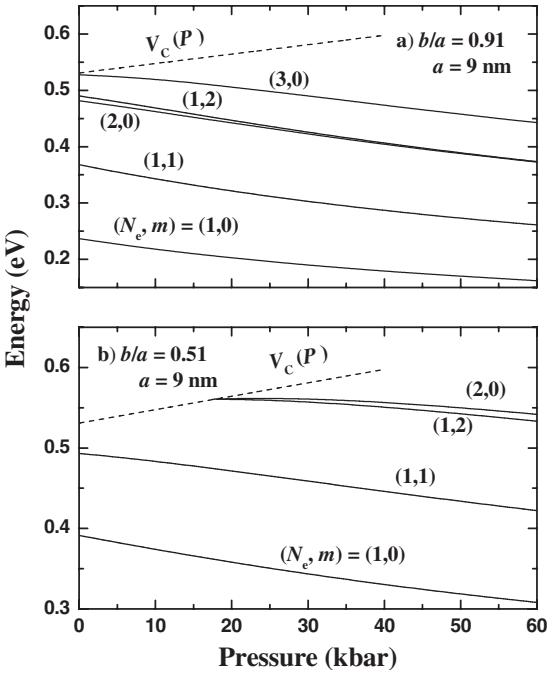

FIG. 3. First energy levels in the conduction band as a function of the pressure. (a) $b/a=0.91$ and $a=9$ nm. (b) $b/a=0.51$ and $a=9$ nm. In both panels the confined potential energy is shown by dashed lines.

to the conduction band states N_e. Only those states with $N_e=N_h$ are shown because they present the stronger values of the OME. The values of the OME corresponding to the transitions with $N_h \neq N_e$ are very small and decrease with pressure. For comparison the transitions from heavy hole valence band are shown by solid lines and from light hole valence band by dashed lines. The configurations used were $a=9$ nm and $b/a=0.91$ while in the inset the same radius is used, but a more confined region with $b/a=0.51$. It can be seen that as the number N increases, the OME value decreases for a given pressure. Nevertheless, the OME for the light hole states has larger value than those corresponding to

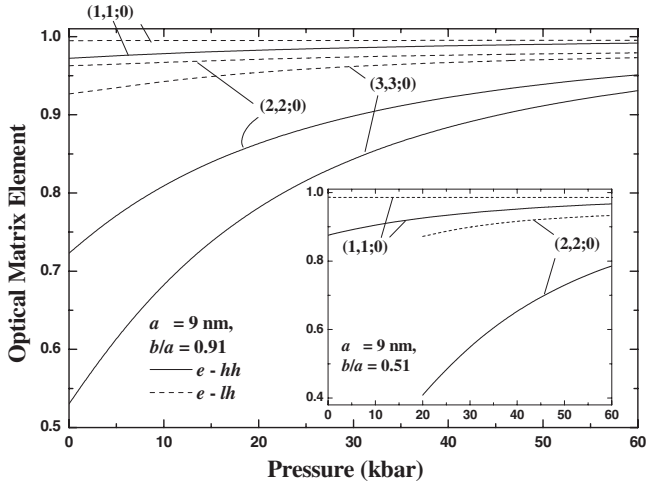

FIG. 4. OME as a function of the pressure for electron-hole transitions $(N_e,N_h;m)$ with $N_e=N_h$ and $m=0$. The transitions from heavy hole states are shown in solid line while from light hole states in dashed lines. The configuration lens is $a=9$ nm with $b/a=0.91$. In the inset the same radius and $b/a=0.51$.

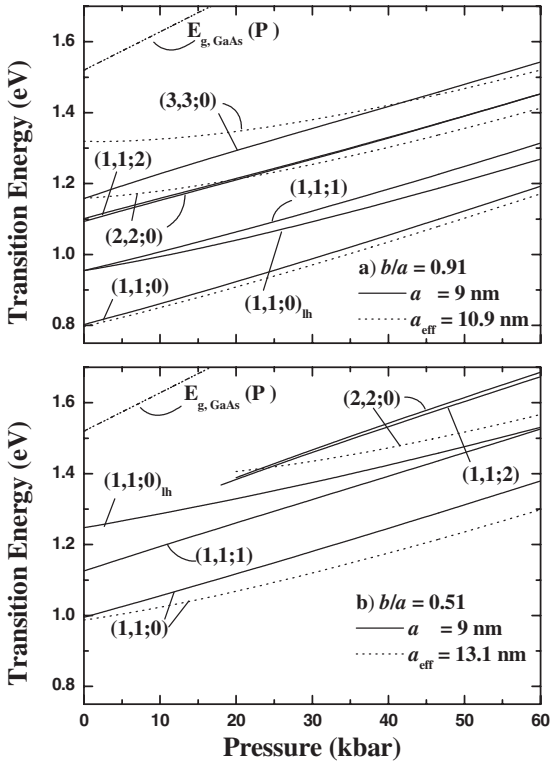

FIG. 5. First allowed optical transition energies of two InAs/GaAs quantum lens as a function of the pressure with $a=9$ nm. (a) $b/a=0.91$ and (b) $b/a=0.51$. Solid lines are obtained by considering finite barrier while dotted lines represent the result with infinite barrier using an effective radius a_{eff} as a fitting parameter at $P=0$.

the heavy hole contributions. From the figure it follows that as the ratio b/a decreases ($b/a=0.51$ in the inset) while keeping the lens radius constant, the value of the OME is reduced. This result is a direct consequence of the spatial confinement. Since the energy levels rise with the confinement (see Fig. 3) the wave functions are less localized and the overlapping of the states with different effective masses decreases. Finally, it can be seen that the OME increases as P increases. Hence, we can conclude that at high pressure the main contribution to the observed PL lines comes from these states with $N_e=N_h$.

Taking into consideration the selection rules obtained above, in Fig. 5 is shown, in solid lines, the variation with the pressure of the first allowed optical transition energies for $N_e=N_h$ and two InAs/GaAs quantum lens configuration. In Fig. 5(a) $b/a=0.91$ is considered while in Fig. 5(b) we have a stronger deformed lens with $b/a=0.51$. In both cases we used $a=9$ nm, $\Delta/R=0.3$, and a 500×500 matrix in the diagonalization procedure. The dashed line is the variation in the energy gap of the GaAs surrounding medium as a function of the pressure. In general, all transitions correspond to the electron-heavy hole states, except $(N_e,N_{lh};m)=(1,1;0)_{lh}$, which corresponds to the electron-light hole state. As can be seen, the values of the transition energy for these states always increase with pressure. This behavior is due to the InAs energy gap dependence on P according to Eq. (2).[33,47] In the case of Fig. 5(b), the stronger confinement provokes an increase in the corresponding energy levels and

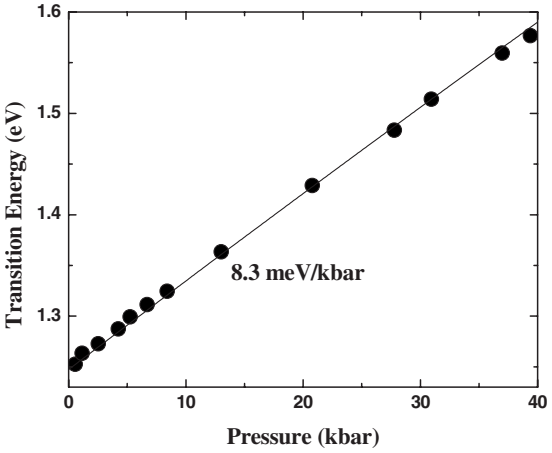

FIG. 6. Ground state transition energy for an InAs/GaAs SAQD structure. Solid circles are data reported in Refs. 28 and 29. Solid line represents the theoretical calculation for a lens shape geometry with radius $a=6.4$ nm at $P=0$ and $b/a=0.34$.

at $P=0$ in the presence of only two transitions, while transitions (1,2;2) and (2,2:0) appear for $P>20$ kbars.

On the other hand, each panel shows, in dotted line, the calculation using the infinite potential barrier model. Here, we introduced an effective radius a_{eff} as a fitting parameter at $P=0$ for the ground transition energy (1,1;0). In Fig. 5(a) the fitting procedure is reasonably good for the electron-hole ground state (1,1;0) for all values of P but it becomes worse for the excited ones. In the case of Fig. 5(b), the implementation of an a_{eff} at $P=0$ does not work properly even for the (1,1;0) transition and it does not have sense for the (2,2;0) electron-hole state transition. This result can be understood by taking into consideration that Fig. 5(b) corresponds to the strong confinement regime and the infinite barrier model breaks down. In the case of a quantum lens with higher values of b/a and radius (soft confinement regime), the energy levels are deep enough in the well. Then, the finite value of the band offset, and its dependence with pressure, will have no appreciable influence on the transition energies and the model of infinite barrier will be suitable in characterizing the system.

IV. COMPARISON WITH EXPERIMENTAL RESULTS

In spite of the limitation of the present simulation we explored its viability by comparing with available experimental data. Figure 6 shows, in solid circles, the experimental transition energy for the electron-hole ground state as a function of the pressure for an InAs/GaAs SAQD reported in Refs. 28 and 29. We have calculated the ground state transition energy ($N_e=1, N_{hh}=1; m=0$) in terms of the applied hydrostatic pressure. To fit the data in our calculation we fixed the ratio $b/a=0.34$ independent of P and used the value of $a=6.4$ nm at $P=0$. The theoretical result is shown in solid line. Note that the value of b/a, but not the radius a, here employed matched very well with the estimation given in Ref. 30.

Notice from Fig. 6 that the value of the linear PC is $dE/dP=8.3$ meV/kbar. In connection with this, the variation in the band offset and the change in the effective masses with P are responsible for the obtained value. Also, it is important to remark that the input used value of the linear PC in Table I for the InAs is linked to the good match between the simulation and the experimental data. If the typical bulk value of 100 meV/kbar for InAs is used the agreement goes down drastically. The consideration of the built-in strain of InAs/GaAs in the framework of two-dimensional layer model is one of the key factors that allow the correct characterization of the fundamental optical emission as function of the hydrostatic pressure.

V. CONCLUSIONS

A model that allows us to include the pressure dependence of the volume, the band offset, and the effective masses in the calculation of the energy levels at the Γ point of the Brillouin zone in SAQDs with lens shape geometry was developed. The importance of the involved parameters on the electronic states and on optical emission for SAQDs under hydrostatic pressure ranging between 0 and 40 kbars was outlined. Also, we have delimited the validity of the infinite potential barrier model for the evaluation of the energy levels as a function of the hydrostatic pressure in quantum lens.

The strong strain effect of InAs/GaAs on the gap energy and PC can be considered under two-dimensional layer approximation guaranteeing a reliable description of the fundamental PL line as a function of the applied pressure.

The present model is a qualitative one which needs to be improved in order to include the more complex effects present in such structures such as the real strain field in dots with lens symmetry, the peculiarity of the valence bands in III-V semiconductors, and excitonic effects.

ACKNOWLEDGMENTS

C.A.D. would like to thank the Colombian COLCIENCIAS Agency and CODI-Universidad de Antioquia for partial financial support. This work has been partially supported by the Excellence Center for Novel Materials (ECNM) under Colciencias Contract No. 043-2005. The author is also grateful to Dr. Anna Kurczyńska for useful discussion. A.H.R. would like to thank Dr. Rubén Barrera Pérez for fruitful comments and the Department of Solid State, Institute of Physics, UNAM, where part of this work was carried out. The authors also thank Dr. Nelson Porras-Montenegro for important discussions.

[1] L. Jacak, P. Hawrylak, and A. Wojs, *Quantum Dots* (Springer-Verlag, Berlin, 1998).
[2] D. Bimberg, M. Grundmann, and N. N. Ledentsov, *The Quantum Dot Heterostructures* (Wiley, Chichester, 1999).
[3] M. A. Cusack, P. R. Briddon, and M. Jaros, Phys. Rev. B **54**, R2300 (1996).
[4] M. A. Cusack, P. R. Briddon, and M. Jaros, Phys. Rev. B **56**, 4047 (1997).
[5] M. Grundmann, O. Stier, and D. Bimberg, Phys. Rev. B **52**, 11969 (1995).
[6] L. Wang and A. Zunger, Phys. Rev. B **59**, 15806 (1999).
[7] C. Pryor, Phys. Rev. B **57**, 7190 (1998).
[8] O. Stier, M. Grundmann, and D. Bimberg, Phys. Rev. B **59**, 5688 (1999).
[9] A. Zunger, Phys. Status Solidi B **224**, 727 (2001).
[10] M. Roy and P. A. Maksym, Phys. Rev. B **68**, 235308 (2003).
[11] A. Wojs, P. Hawrylak, S. Fafard, and L. Jacak, Phys. Rev. B **54**, 5604 (1996).

[12]D. J. Eaglesham and M. Cerullo, Phys. Rev. Lett. **64**, 1943 (1990).
[13]A. Forchel, R. Steffen, T. Koch, M. Michel, M. Albrecht, and T. L. Reinecke, Semicond. Sci. Technol. **11**, 1529 (1996).
[14]I. Hapke-Wurst, U. Zeitier, H. W. Schumacher, R. J. Haug, K. Pierz, and F. J. Ahlers, Semicond. Sci. Technol. **14**, L41 (1999).
[15]J. H. Zhu, K. Brunner, and G. Abstreiter, Appl. Phys. Lett. **72**, 424 (1998).
[16]X. Z. Liao, J. Zou, X. F. Duan, D. J. H. Cockayne, R. Leon, and C. Lobo, Phys. Rev. B **58**, R4235 (1998).
[17]J. M. Moison, F. Houzay, F. Barthe, L. Leprince, E. Andre, and O. Vatel, Appl. Phys. Lett. **64**, 196 (1994).
[18]A. H. Rodríguez, C. Trallero-Giner, S. E. Ulloa, and J. Marín-Antuña, Phys. Rev. B **63**, 125319 (2001).
[19]J. Zou, X. Z. Liao, D. J. H. Cockayne, and R. Leon, Phys. Rev. B **59**, 12279 (1999).
[20]J. Even and S. Loualiche, J. Phys. A **36**, 11677 (2003).
[21]C. Y. Ngo, S. F. Yoon, and W. J. Fan, Phys. Rev. B **74**, 245331 (2006).
[22]L. C. L. Y. Voon and M. Willatzen, J. Phys.: Condens. Matter **14**, 13667 (2002).
[23]A. H. Rodríguez and L. Meza-Montes, Phys. Status Solidi B **243**, 1276 (2006).
[24]N. Y. Tang, X. S. Chen, and W. Lu, Phys. Lett. A **336**, 434 (2005).
[25]F. J. Manjón, A. R. Goñi, K. Syassen, F. Heinrichsdorff, and C. Thomsen, Phys. Status Solidi B **235**, 496 (2003).
[26]C. Kristukat, A. R. Goñi, K. Potschke, D. Bimberg, and C. Thomsen, Phys. Status Solidi B **244**, 53 (2007).
[27]J.-W. Luo, S.-S. Li, and J.-B. Xia, Phys. Rev. B **71**, 245315 (2005).
[28]I. E. Itskevich, M. Henini, H. A. Cardona, L. Eaves, P. C. Main, D. K. Maude, and J. C. Portal, Appl. Phys. Lett. **70**, 505 (1997).
[29]I. E. Itskevich, S. G. Lyapin, I. A. Troyan, P. C. Klipstein, L. Eaves, P. C. Main, and M. Henini, Phys. Rev. B **58**, R4250 (1998).
[30]I. E. Itskevich, M. S. Skolnick, D. J. Mowbray, I. A. Troyan, S. G. Lyapin, L. R. Wilson, M. J. Steer, M. Hopkinson, L. Eaves, and P. C. Main, Phys. Rev. B **60**, R2185 (1999).
[31]B. S. Ma, X. D. Wang, F. H. Su, Z. L. Fang, K. Ding, Z. C. Niu, and G. H. Li, J. Appl. Phys. **95**, 933 (2004).
[32]A. M. Mintairov, K. Sun, J. L. Merz, C. Li, A. S. Vlasov, D. A. Vinokurov, V. Tokranov, and S. Oktyabrsky, Phys. Rev. B **69**, 155306 (2004).
[33]C. A. Duque, N. Porras-Montenegro, Z. Barticevic, M. Pacheco, and L. E. Oliveira, J. Phys.: Condens. Matter **18**, 1877 (2006).
[34]M. D. Frogley, J. R. Downers, and D. J. Dunstan, Phys. Rev. B **62**, 13612 (2000).
[35]Z. M. Fang, K. Y. Ma, D. H. Jaw, R. M. Cohen, and G. B. Stringfellow, J. Appl. Phys. **67**, 7034 (1990).
[36]C. Trallero-Giner, K. Kunc, and K. Syassen, Phys. Rev. B **73**, 205202 (2006).
[37]A. H. Rodríguez, C. Trallero-Giner, M. Muñoz, and M. C. Tamargo, Phys. Rev. B **72**, 045304 (2005).
[38]A. H. Rodríguez, C. R. Handy, and C. Trallero-Giner, J. Phys.: Condens. Matter **15**, 8465 (2003).
[39]A. H. Rodríguez and C. Trallero-Giner, J. Appl. Phys. **95**, 6192 (2004).
[40]R. Courant and D. Hilbert, *Methods of Mathematical Physics* (Interscience, New York, 1953).
[41]S. Le Goff and B. Stébé, Phys. Rev. B **47**, 1383 (1993).
[42]We have evaluated the influence of the built-in strain in InAs dots on the band gap following the treatments of strained layers reported in Ref. 33.
[43]The band-gap linear pressure coefficients were evaluated according to the nonlinear elasticity theory following Refs. 31 and 33. This treatment explains the lower value of the α coefficient for strained InAs relative to the unstrained bulk value. The model assumes a simple strain two-dimensional layer.
[44]*Landolt Börnstein Tables*, Landolt-Börnstein New Series, edited by O. Madelung, Group III, Vol. 37a (Springer-Verlag, Berlin, 1982).
[45]V. López-Richard, G. E. Marques, C. Trallero-Giner, and J. Drake, Phys. Rev. B **58**, 16136 (1998).
[46]C. Trallero-Giner, A. Alexandrou, and M. Cardona, Phys. Rev. B **38**, 10744 (1988).
[47]A. H. Rodríguez, C. A. Duque, C. Trallero-Giner, G. J. Vázquez, M. del Castillo-Mussot, and N. Porras-Montenegro, Phys. Status Solidi B **244**, 48 (2007).